1 **Dry and warm conditions in Australia exacerbated by aerosol reduction in China**

2

3

4

5

6 Jiyuan Gao[1], Yang Yang[1*], Hailong Wang[2], Pinya Wang[1], Hong Liao[1]

7

8

9

10

11

12

13

14 [1]Joint International Research Laboratory of Climate and Environment Change (ILCEC), Jiangsu

15 Key Laboratory of Atmospheric Environment Monitoring and Pollution Control, Jiangsu

16 Collaborative Innovation Center of Atmospheric Environment and Equipment Technology,

17 School of Environmental Science and Engineering, Nanjing University of Information Science

18 and Technology, Nanjing, Jiangsu, China

19 [2]Atmospheric, Climate, and Earth Sciences Division, Pacific Northwest National Laboratory,

20 Richland, Washington, USA

21

22

23

24

25

26 *Correspondence to yang.yang@nuist.edu.cn

27

28 **Abstract**

29 A substantial decline in anthropogenic aerosols in China has been observed since the initiation of

30 clean air actions in 2013. Concurrently, Australia experienced anomalously dry and warm

31 conditions since the 2010s. This study reveals a linkage between aerosol reductions in China and

32 the drying and warming trends in Australia during 2013–2019 based on fully-coupled climate

33 model simulations and multi-source observations. Aerosol decline in China triggered alterations

34 in temperature and pressure gradients between the two hemispheres, leading to intensified outflow

35 from Asia towards the South Indian Ocean, strengthening the Southern Indian Subtropical High

36 and its related Southern Trade Winds. Consequently, this atmospheric pattern resulted in a

37 moisture divergence over Australia. The reduction in surface moisture further resulted in more

38 surface energy being converted into sensible heat instead of evaporating as latent heat, warming

39 the near-surface air. Aerosol reductions in China are found to contribute to 19% of the observed

40 decreases in precipitation and relative humidity and 8% of the increase in surface air temperature

41 in Australia during 2013–2019. The intensified dry and warm climate conditions during 2013–

42 2019 further explain 12%–19% of the increase in wildfire risks during fire seasons in Australia.

43 Our study illuminates the impact of distant aerosols on precipitation and temperature variations in

44 Australia, offering valuable insights for drought and wildfire risk mitigation in Australia.

45

1 Introduction

Australia encompasses various climate zones, ranging from the tropical climate in the north to arid conditions in the interior and temperate climates in the south (Head et al., 2014). The continent is predominantly dry, receiving an average annual rainfall of less than 600 mm and less than 300 mm over half of the land. Evident long-term trends can be observed in Australia's historical rainfall records. These trends reveal a notable shift towards drier conditions across southern Australia (Dey et al., 2019a; Nicholls, 2006; Rauniyar and Power, 2020; Wasko et al., 2021), and an increase in rainfall before 2010 (Dey et al., 2019a, b; Evans et al., 2014; Nicholls, 2006; Rotstayn et al., 2007; Wasko et al., 2021) followed by a slight decreasing trend of rainfall after 2010 (CSIRO and BOM, 2022) in the northern Australia.

Precipitation in Australia is influenced by a variety of atmospheric circulation systems, including East Coast Lows (ECLs), the Australian-Indonesian Monsoon, tropical cyclones (TCs), fronts, and different modes of large-scale climate variabilities, such as the El Niño-Southern Oscillation (ENSO), Indian Ocean Dipole (IOD), Interdecadal Pacific Oscillation (IPO), Subtropical ridge (STR), Southern Annular Mode (SAM), and Madden Julian Oscillation (MJO) (Dey et al., 2019a; Risbey et al., 2009). The linkages between Australia's rainfall characteristics and these drivers could change in response to the internal natural variabilities and external anthropogenic forcings. Rauniyar and Power (2020) reported that the drier conditions across the southern Australia could be attributed to a combination of both decadal-scale natural variability and changes in large-scale atmospheric circulation patterns, which was linked to the escalating emissions of greenhouse gases (GHGs), while Rotstayn et al. (2007) found that the increased levels of rainfall in northern Australia before 2010 was linked to the increases in aerosols in Asia.

Human activities have led to a rise of global surface air temperature by approximately 1.29 °C (0.99 to 1.65 °C) from 1750 to 2019, mainly due to an enhanced greenhouse effect from increasing GHG emissions (IPCC, 2021). In addition to GHGs, human activities also emit a variety of aerosols and their gaseous precursors into the atmosphere. Since industrialization, there has been a significant rise in the levels of aerosols and precursors (Hoesly et al., 2018). Atmospheric aerosols are the second-largest anthropogenic climate forcer, exerting an overall cooling effect that partially masks the warming induced by GHGs. (IPCC, 2013, 2021). However, as anthropogenic

75   aerosols declined during the past decades in many countries of the world related to the clean air

76   actions, the associated "unmask" effect is likely to exacerbate GHG-induced warming (Kloster et

77   al., 2010). For example, in the 1980s, clean air actions were implemented in North America and

78   Europe, leading to a decrease in the emissions of aerosols and their precursors (Hoesly et al., 2018).

79   Reductions in aerosol emissions in the U.S. have led to changes in aerosol direct radiative forcing

80   (DRF) by 0.8 W m^{-2} and indirect radiative forcing (IRF) by 1.0 W m^{-2} over the eastern U.S. during

81   1980–2010 (Leibensperger et al., 2012). Similarly, aerosol decreases over Europe between the

82   1980s and 1990s have caused a change in regional DRF by 1.26 W m^{-2} (Pozzoli et al., 2011). In

83   China, the emissions of aerosols and their precursors have been reduced since 2013 due to the

84   implementation of Air Pollution Prevention and Control Action Plan. Dang and Liao (2019)

85   reported a 1.18 W m^{-2} change in DRF between 2012 and 2017 due to decreased aerosol levels over

86   eastern China. Gao et al. (2022) estimated a warming of 0.20 °C in China, 0.15 °C in North

87   America, and 0.14 °C in Europe, attributed to the decreases in aerosols during 2013–2019.

88   Monsoonal rainfall serves as a vital resource for agriculture, industry, and ecosystems across

89   the monsoon-affected regions, affecting approximately two-thirds of the world's population (B.

90   Wang et al., 2021). Apart from GHGs-induced warming (Cook and Seager, 2013) and nature

91   variabilities (e.g., ENSO) (Oh and Ha, 2015), aerosol also modulates monsoon system mainly

92   through changing land-sea temperature and pressure gradient. The impact of aerosols on Asian

93   monsoon has been widely investigated. Based on climate model simulations, Liu et al. (2023)

94   found that aerosol reductions in East Asia during 2013–2017 resulted in an approximately 5%

95   increase in the strength of the East Asian summer monsoon (EASM). The EASM is also reported

96   to enhance due to future aerosol reductions from 2000 to 2100 (Wang et al., 2016). Dong et al.

97   (2019) explored the effects of increased aerosol in Asia from 1970s to 2000s on atmospheric

98   circulation and rainfall patterns and found anomalous moisture convergence and increased

99   precipitation over the Maritime continent. Non-Asian aerosols also have an effect on South Asian

100   monsoon rainfall through changes in the interhemispheric temperature gradient and meridional

101   shifts of the Intertropical Convergence Zone (Bollasina et al., 2011, 2014; Cowan and Cai, 2011;

102   Undorf et al., 2018). Australia, especially in northern Australia, is largely affected by the Australian

103   monsoon, which is characterized by winds that blow from the southeast during cold season and

104   from the northwest during the warm season (Gallego et al., 2017; Heidemann et al., 2023).

105   Australia has a relatively low level of anthropogenic aerosols, which suggests that the impact of

106   domestic anthropogenic aerosols on Australian monsoon should not be significant. However, the

107   impact of remote aerosols on Australian monsoon have been investigated in previous studies, and

108   they reported that the increases in Asian aerosols could enhance rainfall in Australia through

109   increasing monsoonal winds towards Australia (Rotstayn et al., 2007; Fahrenbach et al., 2023).

110   Wildfires, which are uncontrolled fires spreading rapidly across natural landscapes, are

111   significantly influenced by meteorological conditions (He et al., 2019; Jones et al., 2022). In

112   Australia, these fires, also known as bushfires, present a major environmental and social threat

113   (Johnston et al., 2021; Ward et al., 2020). According to Dowdy (2020), the most favorable seasons

114   for wildfires in most regions of Australia are austral spring and summer. Key meteorological

115   factors such as extended periods of drought, elevated temperatures, low humidity, and strong winds

116   are crucial in determining the occurrence and intensity of wildfires (Zacharakis and Tsihrintzis,

117   2023). Under the recent historical climate change, Australia has witnessed a rise in extreme fire

118   weather conditions and an extended fire season (CSIRO and BOM, 2022).

119   Since the implementation of clean air policies in 2013, there has been a noticeable decrease

120   in aerosol levels in China (Zhang et al., 2019; Zheng et al., 2018). Numerous studies have shown

121   the local and global climate effects of the aerosol reductions in China (Dang and Liao, 2019; Gao

122   et al., 2022, 2023; Liu et al., 2023; Zheng et al., 2020). The Australian monsoonal wind patterns,

123   reported to be influenced by Asian aerosol emissions in the past decades (Rotstayn et al., 2007;

124   Fahrenbach et al., 2023), may have also influenced by the radiative effects due to the aerosol

125   decline in China. The objective of this study is to assess the worsened dry and warm conditions

126   and associated wildfire risk in Australia during 2013–2019 and investigate the possible linkage

127   between the changes in climate conditions in Australia and anthropogenic aerosols.

128   **2 Methods**

129   **2.1 Observational and Reanalysis Data**

130   Ground-based observational data of near-surface $PM_{2.5}$ concentrations in China 2013–2019

131   are acquired from the China National Environmental Monitoring Centre (CNEMC), which offers

132   daily records of near-surface air pollutant concentrations for nearly 1800 sites. Aerosol Optical

133   Depth (AOD) data are obtained from the Moderate Resolution Imaging Spectroradiometer

134   (MODIS) Deep Blue retrieval (Hsu et al., 2013). These observational data are used for evaluating
135   the performance of model simulated aerosols.

136   ERA5, the fifth generation of the European Centre for Medium-range Weather Forecasts
137   (ECMWF) atmospheric reanalysis, is a comprehensive dataset that provides a detailed and globally
138   consistent view of the earth's atmospheric conditions over the past several decades (Hersbach et
139   al., 2020). In this study, ERA5 data are employed to evaluate the climate condition in Australia
140   and analyze its linkage with aerosol reductions in China during the 2013–2019 by using the 2-
141   meter temperature, total precipitation, relative humidity, cloud cover, wind fields, vertical velocity,
142   surface latent and sensible heat flux, and surface and top of the atmosphere (TOA) solar and
143   longwave radiative flux under both clear and all sky conditions.

144   Clouds and the Earth's Radiant Energy System-Energy Balanced and Filled (CERES-EBAF)
145   is a dataset that provides information on the earth's radiation budget, including surface and TOA
146   energy fluxes (Loeb et al., 2018). It combines data from satellite instruments to estimate how much
147   energy the earth receives from the sun and how much is reflected back to space, helping to
148   understand climate change and energy balance processes. The variables used in the study include
149   cloud cover and surface and TOA solar and longwave radiative fluxes under both clear and all sky
150   conditions.

151   The Global Precipitation Measurement (GPM) mission is a joint initiative by National
152   Aeronautics and Space Administration (NASA) and the Japan Aerospace Exploration Agency
153   (JAXA) aimed at providing accurate and frequent measurements of global precipitation
154   (Skofronick-Jackson et al., 2017). GPM includes a core satellite equipped with advanced radar and
155   microwave sensors, enabling the observation of rain and snowfall in real-time. The data are crucial
156   for understanding weather patterns, climate dynamics, and hydrological processes. Precipitation
157   rate data from GPM are also used in the study. GPM provides higher temporal and spatial
158   resolution data compared to Global Precipitation Climatology Project (GPCP), making it more
159   suitable for studies focused on short-term precipitation variability and regional climate dynamics.

2.2 Model Description and Experimental Design

In this research, we conduct simulations to explore the impact of aerosols on climate using the Community Earth System Model version 1 (CESM1). CESM1 simulates the major aerosols including sulfate, black carbon (BC), primary organic matter (POM), secondary organic aerosol (SOA), dust and sea salt in a four-mode Modal Aerosol Module (MAM4), as described in Liu et al. (2016). CESM1 simulations are carried out with 30 vertical layers and a horizontal resolution of 2.5° longitude by 1.9° latitude. In addition to the default model physics, several supplementary features are incorporated into the model in this study to improve the model's performance in simulating aerosol wet scavenging and convective transport (Wang et al., 2013).

The global anthropogenic emissions of aerosols and their precursors are obtained from the Community Emissions Data System (CEDS) v_2021_04_21. In contrast to the prior CEDS v_2016_07_26, which exhibits significant regional emission biases (Z. Wang et al., 2021), the newer CEDS version of anthropogenic emissions of aerosols and precursors considers the substantial reductions in emissions in China, related to the recent clean air actions since 2013 (Fig. S1). Specifically, anthropogenic sulfur dioxide (SO$_2$), BC, and organic carbon (OC) emissions decreased by −12.48, −0.30, and −0.21 Tg yr^{-1}, respectively, over China between 2013 and 2019. Biogenic emissions are from the Model of Emissions of Gases and Aerosols from Nature version 2.1 (MEGAN v2.1) (Guenther et al., 2012), while the emissions from open biomass burning are derived from the CMIP6 (Coupled Model Intercomparison Project Phase 6) (Van Marle et al., 2017).

A series of model experiments are conducted using CESM1 with a fully-coupled model configuration, as detailed in Table S1. In the baseline scenario (referred to as BASE), anthropogenic emissions of aerosols and precursors are fixed at year 2013 worldwide. In CHN, anthropogenic emissions of aerosols and precursors over China are fixed at year 2019, while emissions in all other regions are remained at year 2013. In NAEU, the simulation is performed with anthropogenic emissions of aerosols and precursors over North America and Europe set at year 2019, while emissions in other regions remained at year 2013. In OTH, anthropogenic emissions of aerosols and precursors in other regions except for China are set at year 2019, while emissions in China are kept at year 2013. Biogenic and biomass burning emissions worldwide in

189   all experiments are fixed at year 2013. To reduce model biases related to internal variability, three

190   ensemble members are conducted by perturbing the initial atmospheric temperature conditions.

191   All simulations are run for 150 years, with the last 100 years for detailed analysis.

192   **2.3 Model Evaluation**

193   To validate whether CESM1 can reproduce the aerosol reductions in China during the 2010s,

194   changes in simulated near-surface $PM_{2.5}$ concentrations (sum of sulfate, BC, POM, SOA, dust×0.1,

195   and sea-salt×0.25 following Turnock et al. (2020)) in China during 2013–2019 are compared with

196   the observations. Figure S2 shows spatial distributions of observed and modeled annual mean near-

197   surface $PM_{2.5}$ concentration changes over China (2017–2019 minus 2013–2015), which exhibited

198   a statistically significant correlation coefficient of 0.52 between simulations and observations.

199   However, the model underestimates the $PM_{2.5}$ concentration changes by 76% in China. The

200   considerable underestimation has been reported in many previous studies, resulting from coarse

201   model resolution, uncertainties in emissions of aerosols and precursor gases, strong aerosol wet

202   removal, and the model's deficiency in simulating nitrate and ammonium aerosols (Fan et al.,

203   2018, 2022; Gao et al., 2022, 2023; Zeng et al., 2021). The model has a good capability in

204   replicating the spatial distribution of AOD changes in China during 2013–2019 (Fig. S3), as

205   evidenced by a high correlation coefficient of 0.83, but the model also exhibits an underestimation

206   in the AOD reductions by 69%.

207   Climate variables, including precipitation rate, surface air temperature, relative humidity,

208   total cloud cover, surface solar radiation, 10m wind speed, and surface and TOA net total radiative

209   fluxes under both clear and all sky conditions over Australia simulated by CESM1 model are also

210   compared with those from ERA5 reanalysis (Fig. S4–S6). The model demonstrates a good

211   performance in simulating Australian climate, with normalized mean bias (NMB) values

212   consistently below or near 40% for surface air temperature, relative humidity, total cloud cover,

213   surface downward solar radiation, and 10m wind speed, and surface and TOA net total radiative

214   fluxes, but it tends to overestimate annual precipitation by about 90%, especially over coastal

215   regions likely related to the coarse model resolution. The model accurately reproduces spatial

216   patterns of all climate variables, closely aligning with observations, as indicated by correlation

217   coefficients ranging from 0.7 to 1.0.

218   **2.4 Wildfire Risk Indices**

219   In this study, several climatological indices are used to indicate wildfire risk during fire

220   seasons (austral spring and summer, from September to February of the next year) in Australia

221   (Ren et al., 2022; Irmak et al., 2003; Seager et al., 2015; Sharples et al., 2009).

222   (i) Reference Potential Evapotranspiration (ET_0):

223   ET_0 is a climatological index used to estimate the amount of water that could potentially

224   evaporate and be transpired from the Earth's surface under specific meteorological conditions. The

225   calculation of ET_0 takes into account factors such as temperature (T, unit: °C), and surface

226   downward solar radiation (R_s, unit: W m^{-2}) to estimate the maximum amount of water loss due to

227   evaporation and transpiration. ET_0 is important in wildfire studies because it helps to gauge the

228   environmental moisture conditions and the potential for drought, which can be a significant factor

229   in wildfire risks assessment. ET_0 is given by the following expression (Irmak et al., 2003):

$$ET_0 = -0.611 + 0.149R_s + 0.079\text{T}$$

230

231   (ii) Vapor Pressure Deficit (VPD):

232   Vapor Pressure Deficit (VPD) is a meteorological parameter that measures the difference

233   between the amount of moisture in the air and the maximum amount of moisture the air can hold

234   at a given temperature (T, unit: °C) and moisture (relative humidity, RH, unit: %). High VPD

235   values indicate that the air is dry. VPD is important in the context of wildfires because it reflects

236   the drying potential of the atmosphere. When VPD is high, it can lead to rapid moisture loss from

237   vegetation, making it more susceptible to ignition and increasing the risk of wildfires. VPD is

238   given by (Seager et al., 2015):

$$VPD = \frac{100 - RH}{100} \times 610.7 \times 10^{\frac{7.5T}{237.3+T}}$$

239

240   (iii) McArthur Forest Fire Danger Index (FFDI):

241   The McArthur Forest Fire Danger Index (FFDI) is a widely used index in Australia to assess

242   the potential for bushfires and forest fires. It takes into account various meteorological factors,

243 including T (unit: °C), RH (unit: %), wind speed (U, unit: m s^{-1}), and drought factor (DF, unitless).

244 We set DF as 10 here following Sharples et al. (2009), as it would not significantly affect the

245 methods of comparison used later in their study. While we acknowledge that this assumption is

246 idealized, we find it applicable in our case. To verify this, we calculated gridded DFs for Australia

247 (Figure S7), which show that the DFs are close to 10 and exhibit nearly homogeneous spatial

248 distributions. As such, setting DF = 10 for Australia is reasonable for our analysis. In addition,

249 FFDI calculated using DF = 10 and FFDI using gridded DFs are compared (Figure S8). The

250 patterns and regional averages of both datasets are very similar, further supporting the use of DF

251 = 10 in our study. The FFDI provides a numerical rating that indicates the level of fire danger,

252 with higher values corresponding to greater fire risks. This index is particularly valuable for

253 assessing the immediate risk of wildfires and is commonly used in fire management and prediction.

254 FFDI is defined as (Sharples et al., 2009):

$$FFDI = 2e^{-0.45+0.987lnDF+0.0338T-0.0345RH+0.0234U}$$

255

3 Results

256

3.1 Intensified Dry and Warm Conditions in Australia by aerosol changes

257

258   Figure 1 shows simulated responses in annual precipitation rate, surface air temperature and

259 relative humidity in Australia to changes in anthropogenic emissions of aerosols and precursors.

260 In response to aerosol reductions in China, Australia experiences significant decreases in

261 precipitation and relative humidity, while the temperature has an increase from 2013 to 2019. On

262 regional average, annual precipitation, surface air temperature and relative humidity change by –

263 0.10 mm day^{-1}, 0.08 °C, and –1.19%, respectively, in Australia caused by the aerosol reduction in

264 China during this time period, contributing to the dry and warm climate in Australia. Notably,

265 Northern Australia experiences the most significant reduction in convective precipitation, whereas

266 Southern Australia has the greatest decline in large-scale precipitation related to the aerosol

267 reduction in China, as simulated by the CESM1 model (Fig. S9). The direction of seasonal

268 responses in precipitation rate, surface air temperature and relative humidity are the same as the

269 annual averages, with the largest changes occurring in austral spring (Fig. 2).

270   The intensified dry and warm conditions in Australia can also be seen in the observations,

271   as indicated by ERA5 reanalysis data (Fig. 3). Since 2010, precipitation and relative humidity have

272   significantly decreased in Australia, especially in Northern and Eastern Australia, at a rate of 0.086

273   mm day^{-1} yr^{-1} and 1.07% yr^{-1}, respectively, while surface air temperature has increased at a rate

274   of 0.17 °C yr^{-1}. Note that, the trends in observations are calculated during 2010–2019 to minimize

275   the internal variability. The decrease in precipitation in Australia is also reflected in the GPM data

276   (Fig. S10). It translates into the changes in precipitation, temperature and relative humidity by 0.52

277   mm day^{-1}, 1.0 °C and 6.4% in Australia during 2013–2019 in observations if the trends are

278   assumed to be linear. This suggests that aerosol reductions in China can explain 19% of the

279   decreases in precipitation and relative humidity and 8% of the increase in surface air temperature

280   in Australia during 2013–2019, worsening the dry and warm climate conditions in Australia (Fig.

281   S11). However, considering that aerosols are underestimated in the model, the impact of aerosol

282   reductions in China on Australia's climate may also be underestimated. The reduction in

283   anthropogenic SO_2 emissions in China shows strong correlations with the decrease in precipitation

284   and the increase in temperature in Australia during 2010–2019 (Fig. S12). However, when

285   extending the time frame to the period before emissions reductions in China (1940–2019), the

286   increase in temperature becomes less pronounced, with a slight rise in precipitation and relative

287   humidity, likely attributed to greenhouse gas warming, which can serve as indication that the

288   decrease in precipitation and increase in temperature in Australia from 2010 to 2019 are not

289   primarily caused by GHGs (Figure S13). The rainfall decrease is consistent with changes in clouds.

290   Spatial distributions of simulated changes in vertically-integrated cloud cover and the linear trends

291   in observations are shown in Fig. S14–S16. In both observation and model simulation, the results

292   consistently indicate a reduction in clouds of all levels, including high, mid-level, and low clouds.

293   In addition, the spatial distributions of these changes closely resemble the patterns of responses in

294   precipitation and relative humidity.

295   Aerosol emissions have changed across the world rather than in China alone during 2013–

296   2019, such as those in Australia, North America and Europe, which affect climate in both local

297   and remote regions. Figure 1 also shows changes in climate variables in Australia due to changes

298   in other regions except China. The aerosol changes in other regions except China yield a decrease

299   in precipitation by 0.05 mm day^{-1}, an increase in temperature by 0.08 °C and a decrease in relative

300   humidity by 0.67%. In particular, North America and Europe emission changes, to some extent,

301 contribute to the responses in precipitation (–0.04 mm day^{-1}), temperature (0.08 °C) and relative

302 humidity (–0.33%) attributed to other regions (except China), although the responses are mostly

303 insignificant (Fig. 1).

3.2 Mechanisms of Dry and Warm conditions in Australia Amplified by Aerosol Reductions
in China

306 The rising levels of Asian aerosols could influence the meridional temperature and pressure

307 gradients across the Indian Ocean and therefore affect monsoonal winds and rainfall in Australia

308 since the middle of the 20th century, as reported in several previous studies (Fahrenbach et al.,

309 2023; Rotstayn et al., 2007). Since 2013, aerosol levels in China have substantially decreased due

310 to clean air actions initiated by the Chinese government (Zhang et al., 2019). At the same time,

311 precipitation in Australia exhibited a declining trend, which could be partly attributed to the

312 decrease in China's anthropogenic aerosol forcing as quantified through CESM1 simulations.

313 Asian monsoon region is closely connected with the meridional Hadley circulation and zonal

314 Walker circulation through monsoon outflow to the South India ocean subtropical high (SISH) and

315 North Pacific subtropical high (NPSH) (Beck et al., 2018). Figure 4a illustrates the climatological

316 mean wind fields at 850 hPa, indicating the persistent existence of SISH in the Indian Ocean and

317 NPSH in the North Pacific. With reductions in aerosols in China, the sea surface temperature (SST)

318 increases in the North Pacific but decreases in the Indian Ocean (Fig. 4b), which is concurrent with

319 the northward shift of the Intertropical Convergence Zone (ITCZ) (Basha et al., 2015). Over Asia,

320 this migration of ITCZ is accompanied by the northward movement of the upper-tropospheric

321 subtropical zonal westerly jet (Chiang et al., 2015; Schiemann et al., 2009), which moves to the

322 north of the Tibetan Plateau. It then enhances the circulation pattern of the Tibetan high, redirects

323 the outflow from the Asian monsoon to the southern Indian Ocean subtropical high (Fig. 5c),

324 strengthens the SISH, and leads to the enhancement of the Southern Trade Winds (Fig. 5d). On

325 the other hand, the increase in SST in the North Pacific induces ascending motion around the 130°–

326 150°E and the subsequent descending motion around the 90°–110°E (Fig. 5b), with anomalous

327 westerly winds near the surface, leading to a weakening of NPSH along with a decrease in the

328 Northern Trade Winds (Fig. 5d). Note that, the descending motion partly compensates the

329 ascending motion related to the meridional circulation between 10°–30°N (Fig. 5c). Although only

330 a few significant changes persist in Northern Australia, the observed large-scale circulations

331 around Australia show noticeable similarities to the simulated results (Fig. S17). The mechanism

332 of China's aerosol reductions on the large-scale 3D circulation in the Asia-Pacific region is shown

333 in Figure 6. The enhancement of the Southern Trade Winds further causes moisture advection

334 away from Australia, accompanied by moisture divergence in Australia, especially over the

335 northern Australia (Fig. S18). Moisture divergence is also evident in the observations for some

336 northern regions of Australia (Fig. S19). This moisture divergence in Australia then intensifies the

337 dryness in Australia both in CESM1 simulations (Fig. 1) and ERA5 reanalysis (Fig. 3).

338 Figures 7 illustrate the changes in relevant radiative fluxes in Australia resulting from

339 aerosol changes in China. Under the clear sky condition, both surface and top of the atmosphere

340 (TOA) radiative flux decrease (Fig. 7c&d). It is due to increased sea salt and dust aerosols (Fig.

341 S20b–d) due to the stronger Southern Trade Winds (Figs. S20a and 5d) and dryer conditions (Fig.

342 1). The decrease in cloud cover (Fig. S14) leads to an overall increase in both surface and TOA

343 radiative flux (Fig. 7e&f). The overall changes in radiative fluxes are offset by these two factors

344 (Fig. 7a&b) and insufficient to explain the significant increase in surface air temperature in

345 Australia (Fig. 1). Similar signals are also evident in the observational data represented by ERA5

346 and CERES-EBAF (Figs. S21 and S22).

347 Decreases in precipitation lead to a decrease in surface specific humidity (Fig. S23a), which

348 declines more than that at 850 hPa (Fig. S23b). This results in excess energy being converted into

349 sensible heat rather than latent heat through evaporation (Chiang et al., 2018; Fischer et al., 2007;

350 Seneviratne et al., 2006; Su et al., 2014), which is indicated by a decrease in surface upward latent

351 heat flux and an increase in surface upward sensible heat flux in Australia due to aerosol changes

352 in China in Figure 8. The increased surface upward sensible heat flux heats the near-surface air

353 and contributes to the warm conditions in Australia. The signals of specific humidity and surface

354 sensible/latent heat flux from ERA5 are consistent with the simulated results. (Figs. S24 and S25).

355 **3.3 Increases in Wildfire Risk in Australia**

356 Wildfires represent a biosphere-atmosphere phenomenon, arising from the intricate interplay

357 of weather, climate, fuels, and human activities (Moritz et al., 2014). Notably, wildfires are ranked

358 among the most significant natural disasters in Australia, causing extensive damage (Shi et al.,

359 2021). Collins et al. (2022) reported that warmer and drier conditions increased the potential for

360 large and severe wildfire in Australia. Given that changes in aerosols in China have led to a warmer

361 and drier climate condition in Australia in recent years, the change in this climate state could also

362 impact on the occurrence of wildfires. Three wildfire risk indices (ET_0, VPD, and FFDI) are

363 selected to assess the risks of wildfires occurrence. Detailed information about the three wildfire

364 risk indices can be found in the Methods section.

365 All three indices exhibit increases (+0.36 mm mon^{-1} for ET_0, +0.56 hPa for VPD, and +0.24

366 for FFDI) during fire seasons (September to February) in Australia due to changes in aerosols in

367 China during 2013–2019 (Fig. 9), although they do not show the same spatial distribution possibly

368 due to different considerations regarding climate variables in the indices. The results analyzed

369 from observational data also exhibit increasing trends at a rate of 0.32 mm mon^{-1} yr^{-1} for ET_0, 0.59

370 hPa yr^{-1} for VPD, and 0.34 yr^{-1} for FFDI during this time period (Fig. S26). It further indicates

371 that the decline in anthropogenic aerosols in China can explain 12%–19% of the increase in

372 wildfire risks during the fire season in Australia between 2013 and 2019 through inducing dry and

373 warm wildfire weather conditions (Fig. S11). However, considering that aerosols are

374 underestimated in the model, the impact of aerosol reductions in China on Australia's wildfire

375 risks may also be underestimated.

376 **4 Conclusions and Discussions**

377 This study reveals a plausible connection between the substantial aerosol reduction in China

378 and drying and warming trends in Australia that happened during the 2010s. Aerosol reductions in

379 China induce changes in temperature and pressure gradients, which lead to an increased outflow

380 from Asia towards the South Indian Ocean, strengthening the SISH and the associated Southern

381 Trade Winds. Consequently, this atmospheric pattern results in moisture divergence over Australia,

382 causing a decrease in humidity and precipitation. The reduction in surface moisture leads to more

383 surface energy being converted into sensible heat, rather than evaporating as latent heat, thereby

384 heating the near-surface air. This perspective sheds light on the influence of distant aerosols on

385 climate in Australia.

386 The CESM1 simulations depict warmer and drier conditions in Australia related to China's

387 aerosol reductions than otherwise, a pattern also evident in observations represented by ERA5.

388   However, it is important to note that China's aerosol reductions only contribute to a portion of the

389   observed warm and dry conditions in Australia. According to the CESM1 simulations, aerosol

390   changes in China account for 19% of the observed decrease in relative humidity and precipitation

391   and 8% of the increase in temperature in Australia throughout the year, and 12%–19% of the

392   increase in wildfire risks during the fire season in Australia during 2013–2019. Given that aerosols

393   are underestimated in the model, the effect of aerosol reductions in China on Australia's climate

394   and wildfire risks might also be underestimated. Nonetheless, air quality and human health

395   improvements owing to aerosol reductions cannot be ignored (Giani et al., 2020; Zheng et al.,

396   2017). In addition, the drying and warming trends in Australia attributed to aerosol reductions

397   should be considered resulting from the rise in long-lived GHGs, while the aerosol reductions

398   unmask the effect rooted in the GHGs (Wang et al., 2023). In addition, other factors such as

399   internal climate variability (Heidemann et al., 2023) appear to have contributed more to the

400   changes in Australia's climate conditions.

401   There are some potential limitations and uncertainties in this study. Firstly, the low bias in

402   simulated aerosol concentrations in CESM1 could potentially lead to an underestimation of the

403   climate responses in Australia, and the extent to which the low bias could influence the results

404   remains unknown. Secondly, our findings are derived from simulations conducted with a single

405   fully-coupled climate model, and it is vital for future research to employ multi-model ensemble

406   simulations to reduce the possibility of model-dependent specific results. While the CMIP6 and

407   PDRMIP (Precipitation Driver Response Model Intercomparison Project) can assist in minimizing

408   such model dependencies, they also present certain drawbacks. Anthropogenic emissions input in

409   CMIP6 inadequately accounts for aerosol reductions resulting from clean air actions in China since

410   2013 (Z. Wang et al., 2021). Additionally, CMIP6 considers aerosol changes globally, making it

411   challenging to isolate effects specifically induced by changes in aerosols in China. The

412   experimental design of PDRMIP, which scales the concentrations of sulfate and BC in Asia to ten

413   times of their present-day levels, is generally idealistic and may not accurately and proportionally

414   represent aerosol changes observed in the real world. Until now, few studies have explored the

415   link between the recent reduction in China's aerosols and the changing climate conditions in

416   Australia. Although Fahrenbach et al. (2023) investigated the connection between increased

417   precipitation in Australia and elevated aerosol levels in Asia since the last century, they focused

418   on the decadal time scale with historical increasing aerosols in Asia. Besides, while this study

419 relies on equilibrium simulations to isolate the forced response to aerosol changes, we

420 acknowledge that transient simulations, which account for time-varying aerosol reductions, would

421 provide a more accurate depiction of the dynamic climate system response. Given that aerosol

422 reductions in China continue to evolve, transient simulations would be more appropriate for

423 capturing the full temporal effects of these changes. Large-ensemble transient simulations are

424 suggested in future studies to better represent the evolving aerosol-climate interactions over time

425 and to enhance the robustness of the findings. Another limitation of this study is that we calculated

426 the relative contribution of aerosol changes in China to the changing climate in Australia by

427 combining model simulations and observational data, which could lead to the inconsistency and

428 introduce biases to the quantitative results. Finally, in addition to aerosols, GHGs also contribute

429 to regional and global climate change. The extent to which GHGs could contribute to weather

430 condition and climate changes in Australia remains unknown, which warrants further investigation.

431 Nonetheless, our study examined the role of China's aerosol reductions in Australia's recent

432 drying and warming trends. Substantial emission reductions will continue in China following the

433 carbon neutral pathway (Yang et al., 2023), while future changes in emissions in South Asia remain

434 uncertain (Samset et al., 2019). Apart from natural climate variabilities that affect the Australian

435 monsoon, further investigation of changes in monsoon precipitation in Australia should also

436 consider the effects of remote aerosol changes simultaneously, which is crucial to effective drought

437 and wildfire management and mitigation in Australia.

438 **Acknowledgments**

Data and Code Availability

Ground-based observed PM$_{2.5}$ concentrations from CNEMC are available at https://quotsoft.net/air/ (last access: September 2024). AOD from MODIS Deep Blue retrieval are available at https://modis.gsfc.nasa.gov/ (last access: September 2024). ERA5 reanalysis data are available at https://cds.climate.copernicus.eu/ (last access: September 2024). CERES-EBAF data are available at https://ceres.larc.nasa.gov/data/#energy-balanced-and-filled-ebaf (last access: September 2024). GPM data are available at https://disc.gsfc.nasa.gov/datasets/GPM_3IMERGM_07/summary?keywords=%22IMERG%20final%22 (last access: September 2024). The source code of CESM is available at https://github.com/ESCOMP/CESM (last access: September 2024). Our model results can be available at https://doi.org/10.5281/zenodo.13682943 (last access: September 2024).

Author Contributions

Y.Y. conceived the research and directed the analysis. J.G. conceived the research, conducted the model simulations, and performed the analysis. All the authors including H.W., P.W., and H. L. discussed the results and wrote the paper.

Competing Interests

At least one of the (co-)authors is a member of the editorial board of Atmospheric Chemistry and Physics. The peer-review process was guided by an independent editor, and the authors also have no other competing interests to declare.

References

Basha, G., Kishore, P., Venkat Ratnam, M., Ouarda, T. B. M. J., Velicogna, I., and Sutterley, T.: Vertical and latitudinal variation of the intertropical convergence zone derived using GPS radio occultation measurements, Remote Sens. Environ., 163, 262–269, https://doi.org/10.1016/j.rse.2015.03.024, 2015.

Beck, J. W., Zhou, W., Li, C., Wu, Z., White, L., Xian, F., Kong, X., and An, Z.: A 550,000-year record of East Asian monsoon rainfall from 10Be in loess, Science, 360, 877–881, https://doi.org/10.1126/science.aam5825, 2018.

473   Boer, M. M., Resco De Dios, V., and Bradstock, R. A.: Unprecedented burn area of Australian
474   mega forest fires, Nat. Clim. Change, 10, 171–172, https://doi.org/10.1038/s41558-020-
475   0716-1, 2020.

476   Bollasina, M. A., Ming, Y., and Ramaswamy, V.: Anthropogenic Aerosols and the Weakening of
477   the South Asian Summer Monsoon, Science, 334, 502–505,
478   https://doi.org/10.1126/science.1204994, 2011.

479   Bollasina, M. A., Ming, Y., Ramaswamy, V., Schwarzkopf, M. D., and Naik, V.: Contribution of
480   local and remote anthropogenic aerosols to the twentieth century weakening of the South
481   Asian Monsoon, Geophys. Res. Lett., 41, 680–687, https://doi.org/10.1002/2013GL058183,
482   2014.

483   Chiang, F., Mazdiyasni, O., and AghaKouchak, A.: Amplified warming of droughts in southern
484   United States in observations and model simulations, Sci. Adv., 4, eaat2380,
485   https://doi.org/10.1126/sciadv.aat2380, 2018.

486   Chiang, J. C. H., Fung, I. Y., Wu, C.-H., Cai, Y., Edman, J. P., Liu, Y., Day, J. A., Bhattacharya,
487   T., Mondal, Y., and Labrousse, C. A.: Role of seasonal transitions and westerly jets in East
488   Asian paleoclimate, Quat. Sci. Rev., 108, 111–129,
489   https://doi.org/10.1016/j.quascirev.2014.11.009, 2015.

490   Collins, L., Clarke, H., Clarke, M. F., McColl Gausden, S. C., Nolan, R. H., Penman, T., and
491   Bradstock, R.: Warmer and drier conditions have increased the potential for large and severe
492   fire seasons across south-eastern Australia, Glob. Ecol. Biogeogr., 31, 1933–1948,
493   https://doi.org/10.1111/geb.13514, 2022.

494   Cook, B. I. and Seager, R.: The response of the North American Monsoon to increased greenhouse
495   gas forcing, J. Geophys. Res.: Atmos., 118, 1690–1699, https://doi.org/10.1002/jgrd.50111,
496   2013.

497   Cowan, T. and Cai, W.: The impact of Asian and non-Asian anthropogenic aerosols on 20th
498   century Asian summer monsoon: ASIAN MONSOON AND AEROSOLS, Geophys. Res.
499   Lett., 38, L11703, https://doi.org/10.1029/2011GL047268, 2011.

500   CSIRO and BOM: State of the Climate 2022, 2022

501   Dang, R. and Liao, H.: Radiative Forcing and Health Impact of Aerosols and Ozone in China as
502   the Consequence of Clean Air Actions over 2012–2017, Geophys. Res. Lett., 46, 12511–
503   12519, https://doi.org/10.1029/2019GL084605, 2019.

504   Dey, R., Lewis, S. C., Arblaster, J. M., and Abram, N. J.: A review of past and projected changes
505   in Australia's rainfall, WIREs Clim. Change, 10, e577, https://doi.org/10.1002/wcc.577,
506   2019a.

507   Dey, R., Lewis, S. C., and Abram, N. J.: Investigating observed northwest Australian rainfall
508   trends in Coupled Model Intercomparison Project phase 5 detection and attribution
509   experiments, Int. J. Climatol., 39, 112–127, https://doi.org/10.1002/joc.5788, 2019b.

Dong, B., Wilcox, L. J., Highwood, E. J., and Sutton, R. T.: Impacts of recent decadal changes in Asian aerosols on the East Asian summer monsoon: roles of aerosol–radiation and aerosol–cloud interactions, Clim. Dyn., 53, 3235–3256, https://doi.org/10.1007/s00382-019-04698-0, 2019.

Dowdy, A. J.: Seamless climate change projections and seasonal predictions for bushfires in Australia, J. South. Hemisph. Earth Syst. Sci., 70, 120–138, https://doi.org/10.1071/ES20001, 2020.

Evans, S., Marchand, R., and Ackerman, T.: Variability of the Australian Monsoon and Precipitation Trends at Darwin, J. Climate, 27, 8487–8500, https://doi.org/10.1175/JCLI-D-13-00422.1, 2014.

Fahrenbach, N. L. S., Bollasina, M. A., Samset, B. H., Cowan, T., and Ekman, A. M. L.: Asian anthropogenic aerosol forcing played a key role in the multi-decadal increase in Australian summer monsoon rainfall, J. Climate, 1, https://doi.org/10.1175/JCLI-D-23-0313.1, 2023.

Fan, T., Liu, X., Ma, P.-L., Zhang, Q., Li, Z., Jiang, Y., Zhang, F., Zhao, C., Yang, X., Wu, F., and Wang, Y.: Emission or atmospheric processes? An attempt to attribute the source of large bias of aerosols in eastern China simulated by global climate models, Atmos. Chem. Phys., 18, 1395–1417, https://doi.org/10.5194/acp-18-1395-2018, 2018.

Fan, T., Liu, X., Wu, C., Zhang, Q., Zhao, C., Yang, X., and Li, Y.: Comparison of the Anthropogenic Emission Inventory for CMIP6 Models with a Country-Level Inventory over China and the Simulations of the Aerosol Properties, Adv. Atmos. Sci., 39, 80–96, https://doi.org/10.1007/s00376-021-1119-6, 2022.

Fischer, E. M., Seneviratne, S. I., Lüthi, D., and Schär, C.: Contribution of land-atmosphere coupling to recent European summer heat waves, Geophys. Res. Lett., 34, 2006GL029068, https://doi.org/10.1029/2006GL029068, 2007.

Gao, J., Yang, Y., Wang, H., Wang, P., Li, H., Li, M., Ren, L., Yue, X., and Liao, H.: Fast climate responses to emission reductions in aerosol and ozone precursors in China during 2013–2017, Atmos. Chem. Phys., 22, 7131–7142, https://doi.org/10.5194/acp-22-7131-2022, 2022.

Gao, J., Yang, Y., Wang, H., Wang, P., Li, B., Li, J., Wei, J., Gao, M., and Liao, H.: Climate responses in China to domestic and foreign aerosol changes due to clean air actions during 2013–2019, npj Clim. Atmos. Sci., 6, 160, https://doi.org/10.1038/s41612-023-00488-y, 2023.

Giani, P., Castruccio, S., Anav, A., Howard, D., Hu, W., and Crippa, P.: Short-term and long-term health impacts of air pollution reductions from COVID-19 lockdowns in China and Europe: a modelling study, Lancet Planet. Health, 4, e474–e482, https://doi.org/10.1016/S2542-5196(20)30224-2, 2020.

Guenther, A. B., Jiang, X., Heald, C. L., Sakulyanontvittaya, T., Duhl, T., Emmons, L. K., and Wang, X.: The Model of Emissions of Gases and Aerosols from Nature version 2.1

548   (MEGAN2.1): an extended and updated framework for modeling biogenic emissions, Geosci.
549   Model Dev., 5, 1471–1492, https://doi.org/10.5194/gmd-5-1471-2012, 2012.

550 He, T., Lamont, B. B., and Pausas, J. G.: Fire as a key driver of Earth's biodiversity, Biol. Rev.,
551   94, 1983–2010, https://doi.org/10.1111/brv.12544, 2019.

552 Head, L., Adams, M., McGregor, H. V., and Toole, S.: Climate change and Australia, WIREs Clim.
553   Change, 5, 175–197, https://doi.org/10.1002/wcc.255, 2014.

554 Heidemann, H., Cowan, T., Henley, B. J., Ribbe, J., Freund, M., and Power, S.: Variability and
555   long-term change in Australian monsoon rainfall: A review, WIREs Clim. Change, 14, e823,
556   https://doi.org/10.1002/wcc.823, 2023.

557 Hersbach, H., Bell, B., Berrisford, P., Hirahara, S., Horányi, A., Muñoz-Sabater, J., Nicolas, J.,
558   Peubey, C., Radu, R., Schepers, D., Simmons, A., Soci, C., Abdalla, S., Abellan, X., Balsamo,
559   G., Bechtold, P., Biavati, G., Bidlot, J., Bonavita, M., De Chiara, G., Dahlgren, P., Dee, D.,
560   Diamantakis, M., Dragani, R., Flemming, J., Forbes, R., Fuentes, M., Geer, A., Haimberger,
561   L., Healy, S., Hogan, R. J., Hólm, E., Janisková, M., Keeley, S., Laloyaux, P., Lopez, P.,
562   Lupu, C., Radnoti, G., De Rosnay, P., Rozum, I., Vamborg, F., Villaume, S., and Thépaut, J.:
563   The ERA5 global reanalysis, Q. J. R. Meteorol. Soc., 146, 1999–2049,
564   https://doi.org/10.1002/qj.3803, 2020.

565 Hoesly, R. M., Smith, S. J., Feng, L., Klimont, Z., Janssens-Maenhout, G., Pitkanen, T., Seibert,
566   J. J., Vu, L., Andres, R. J., Bolt, R. M., Bond, T. C., Dawidowski, L., Kholod, N., Kurokawa,
567   J., Li, M., Liu, L., Lu, Z., Moura, M. C. P., O'Rourke, P. R., and Zhang, Q.: Historical (1750–
568   2014) anthropogenic emissions of reactive gases and aerosols from the Community Emissions
569   Data System (CEDS), Geosci. Model Dev., 11, 369–408, https://doi.org/10.5194/gmd-11-
570   369-2018, 2018.

571 Hsu, N. C., Jeong, M. -J., Bettenhausen, C., Sayer, A. M., Hansell, R., Seftor, C. S., Huang, J., and
572   Tsay, S. -C.: Enhanced Deep Blue aerosol retrieval algorithm: The second generation, J.
573   Geophys. Res.: Atmos., 118, 9296–9315, https://doi.org/10.1002/jgrd.50712, 2013.

574 Huneeus, N., Denier Van Der Gon, H., Castesana, P., Menares, C., Granier, C., Granier, L.,
575   Alonso, M., De Fatima Andrade, M., Dawidowski, L., Gallardo, L., Gomez, D., Klimont, Z.,
576   Janssens-Maenhout, G., Osses, M., Puliafito, S. E., Rojas, N., Ccoyllo, O. S.-, Tolvett, S., and
577   Ynoue, R. Y.: Evaluation of anthropogenic air pollutant emission inventories for South
578   America at national and city scale, Atmos. Environ., 235, 117606,
579   https://doi.org/10.1016/j.atmosenv.2020.117606, 2020.

580 IPCC: Climate Change 2013: The Physical Science Basis, 2013.

581 IPCC: Climate Change 2021: The Physical Science Basis, 2021.

582 Irmak, S., Irmak, A., Allen, R. G., and Jones, J. W.: Solar and Net Radiation-Based Equations to
583   Estimate Reference Evapotranspiration in Humid Climates, J. Irrig. Drain. Eng., 129, 336–
584   347, https://doi.org/10.1061/(ASCE)0733-9437(2003)129:5(336), 2003.

585 Johnston, F. H., Borchers-Arriagada, N., Morgan, G. G., Jalaludin, B., Palmer, A. J., Williamson,
586   G. J., and Bowman, D. M. J. S.: Unprecedented health costs of smoke-related PM2.5 from
587   the 2019–20 Australian megafires, Nat. Sustain., 4, 42–47, https://doi.org/10.1038/s41893-
588   020-00610-5, 2021.

589 Jones, M. W., Abatzoglou, J. T., Veraverbeke, S., Andela, N., Lasslop, G., Forkel, M., Smith, A.
590   J. P., Burton, C., Betts, R. A., van der Werf, G. R., Sitch, S., Canadell, J. G., Santín, C.,
591   Kolden, C., Doerr, S. H., and Le Quéré, C.: Global and Regional Trends and Drivers of Fire
592   Under Climate Change, Rev. Geophys., 60, e2020RG000726,
593   https://doi.org/10.1029/2020RG000726, 2022.

594 Kloster, S., Dentener, F., Feichter, J., Raes, F., Lohmann, U., Roeckner, E., and Fischer-Bruns, I.:
595   A GCM study of future climate response to aerosol pollution reductions, Clim. Dyn., 34,
596   1177–1194, https://doi.org/10.1007/s00382-009-0573-0, 2010.

597 Lau, K.-M. and Kim, K.-M.: Observational relationships between aerosol and Asian monsoon
598   rainfall, and circulation, Geophys. Res. Lett., 33, 2006GL027546,
599   https://doi.org/10.1029/2006GL027546, 2006.

600 Leibensperger, E. M., Mickley, L. J., Jacob, D. J., Chen, W.-T., Seinfeld, J. H., Nenes, A., Adams,
601   P. J., Streets, D. G., Kumar, N., and Rind, D.: Climatic effects of 1950–2050 changes in US
602   anthropogenic aerosols – Part 1: Aerosol trends and radiative forcing, Atmos. Chem. Phys.,
603   12, 3333–3348, https://doi.org/10.5194/acp-12-3333-2012, 2012.

604 Liu, C., Yang, Y., Wang, H., Ren, L., Wei, J., Wang, P., and Liao, H.: Influence of Spatial Dipole
605   Pattern in Asian Aerosol Changes on East Asian Summer Monsoon, J. Climate, 36, 1575–
606   1585, https://doi.org/10.1175/JCLI-D-22-0335.1, 2023.

607 Liu, X., Ma, P.-L., Wang, H., Tilmes, S., Singh, B., Easter, R. C., Ghan, S. J., and Rasch, P. J.:
608   Description and evaluation of a new four-mode version of the Modal Aerosol Module
609   (MAM4) within version 5.3 of the Community Atmosphere Model, Geosci. Model Dev., 9,
610   505–522, https://doi.org/10.5194/gmd-9-505-2016, 2016.

611 Loeb, N. G., Doelling, D. R., Wang, H., Su, W., Nguyen, C., Corbett, J. G., Liang, L., Mitrescu,
612   C., Rose, F. G., and Kato, S.: Clouds and the Earth's Radiant Energy System (CERES) Energy
613   Balanced and Filled (EBAF) Top-of-Atmosphere (TOA) Edition-4.0 Data Product, J. Climate,
614   31, 895–918, https://doi.org/10.1175/JCLI-D-17-0208.1, 2018.

615 Ming, Y. and Ramaswamy, V.: Nonlinear Climate and Hydrological Responses to Aerosol Effects,
616   J. Climate, 22, 1329–1339, https://doi.org/10.1175/2008JCLI2362.1, 2009.

617 Moritz, M. A., Batllori, E., Bradstock, R. A., Gill, A. M., Handmer, J., Hessburg, P. F., Leonard,
618   J., McCaffrey, S., Odion, D. C., Schoennagel, T., and Syphard, A. D.: Learning to coexist
619   with wildfire, Nature, 515, 58–66, https://doi.org/10.1038/nature13946, 2014.

620 Nicholls, N.: Detecting and attributing Australian climate change: a review, Aust. Meteorol. Mag.,
621   2006.

Oh, H. and Ha, K.-J.: Thermodynamic characteristics and responses to ENSO of dominant intraseasonal modes in the East Asian summer monsoon, Clim. Dyn., 44, 1751–1766, https://doi.org/10.1007/s00382-014-2268-4, 2015.

Pozzoli, L., Janssens-Maenhout, G., Diehl, T., Bey, I., Schultz, M. G., Feichter, J., Vignati, E., and Dentener, F.: Re-analysis of tropospheric sulfate aerosol and ozone for the period 1980–2005 using the aerosol-chemistry-climate model ECHAM5-HAMMOZ, Atmos. Chem. Phys., 11, 9563–9594, https://doi.org/10.5194/acp-11-9563-2011, 2011.

Rauniyar, S. P. and Power, S. B.: The Impact of Anthropogenic Forcing and Natural Processes on Past, Present, and Future Rainfall over Victoria, Australia, J. Climate, 33, 8087–8106, https://doi.org/10.1175/JCLI-D-19-0759.1, 2020.

Ren, L., Yang, Y., Wang, H., Wang, P., Yue, X., and Liao, H.: Widespread Wildfires Over the Western United States in 2020 Linked to Emissions Reductions During COVID-19, Geophys. Res. Lett., 49, e2022GL099308, https://doi.org/10.1029/2022GL099308, 2022.

Risbey, J. S., Pook, M. J., McIntosh, P. C., Wheeler, M. C., and Hendon, H. H.: On the Remote Drivers of Rainfall Variability in Australia, Mon. Wea. Rev., 137, 3233–3253, https://doi.org/10.1175/2009MWR2861.1, 2009.

Rotstayn, L. D., Cai, W., Dix, M. R., Farquhar, G. D., Feng, Y., Ginoux, P., Herzog, M., Ito, A., Penner, J. E., Roderick, M. L., and Wang, M.: Have Australian rainfall and cloudiness increased due to the remote effects of Asian anthropogenic aerosols?, J. Geophys. Res.: Atmos., 112, 2006JD007712, https://doi.org/10.1029/2006JD007712, 2007.

Samset, B. H., Lund, M. T., Bollasina, M., Myhre, G., and Wilcox, L.: Emerging Asian aerosol patterns, Nat. Geosci., 12, 582–584, https://doi.org/10.1038/s41561-019-0424-5, 2019.

Schiemann, R., Lüthi, D., and Schär, C.: Seasonality and Interannual Variability of the Westerly Jet in the Tibetan Plateau Region, J. Climate, 22, 2940–2957, https://doi.org/10.1175/2008JCLI2625.1, 2009.

Seager, R., Hooks, A., Williams, A. P., Cook, B., Nakamura, J., and Henderson, N.: Climatology, Variability, and Trends in the U.S. Vapor Pressure Deficit, an Important Fire-Related Meteorological Quantity, J. Appl. Meteorol. Clim., 54, 1121–1141, https://doi.org/10.1175/JAMC-D-14-0321.1, 2015.

Seneviratne, S. I., Lüthi, D., Litschi, M., and Schär, C.: Land–atmosphere coupling and climate change in Europe, Nature, 443, 205–209, https://doi.org/10.1038/nature05095, 2006.

Sharples, J. J., McRae, R. H. D., Weber, R. O., and Gill, A. M.: A simple index for assessing fire danger rating, Environ. Modell. Softw., 24, 764–774, https://doi.org/10.1016/j.envsoft.2008.11.004, 2009.

Shi, G., Yan, H., Zhang, W., Dodson, J., Heijnis, H., and Burrows, M.: Rapid warming has resulted in more wildfires in northeastern Australia, Sci. Total Environ., 771, 144888, https://doi.org/10.1016/j.scitotenv.2020.144888, 2021.

659 Skofronick-Jackson, G., Petersen, W. A., Berg, W., Kidd, C., Stocker, E. F., Kirschbaum, D. B.,
660   Kakar, R., Braun, S. A., Huffman, G. J., Iguchi, T., Kirstetter, P. E., Kummerow, C.,
661   Meneghini, R., Oki, R., Olson, W. S., Takayabu, Y. N., Furukawa, K., and Wilheit, T.: The
662   Global Precipitation Measurement (GPM) Mission for Science and Society, Bull. Am.
663   Meteorol. Soc., 98, 1679–1695, https://doi.org/10.1175/BAMS-D-15-00306.1, 2017.

664 Streets, D. G., Yan, F., Chin, M., Diehl, T., Mahowald, N., Schultz, M., Wild, M., Wu, Y., and
665   Yu, C.: Anthropogenic and natural contributions to regional trends in aerosol optical depth,
666   1980–2006, J. Geophys. Res.: Atmos., 114, 2008JD011624,
667   https://doi.org/10.1029/2008JD011624, 2009.

668 Su, H., Yang, Z., Dickinson, R. E., and Wei, J.: Spring soil moisture-precipitation feedback in the
669   Southern Great Plains: How is it related to large-scale atmospheric conditions?, Geophys.
670   Res. Lett., 41, 1283–1289, https://doi.org/10.1002/2013GL058931, 2014.

671 Turnock, S. T., Allen, R. J., Andrews, M., Bauer, S. E., Deushi, M., Emmons, L., Good, P.,
672   Horowitz, L., John, J. G., Michou, M., Nabat, P., Naik, V., Neubauer, D., O'Connor, F. M.,
673   Olivié, D., Oshima, N., Schulz, M., Sellar, A., Shim, S., Takemura, T., Tilmes, S., Tsigaridis,
674   K., Wu, T., and Zhang, J.: Historical and future changes in air pollutants from CMIP6 models,
675   Atmos. Chem. Phys., 20, 14547–14579, https://doi.org/10.5194/acp-20-14547-2020, 2020.

676 Undorf, S., Polson, D., Bollasina, M. A., Ming, Y., Schurer, A., and Hegerl, G. C.: Detectable
677   Impact of Local and Remote Anthropogenic Aerosols on the 20th Century Changes of West
678   African and South Asian Monsoon Precipitation, J. Geophys. Res.: Atmos., 123, 4871–4889,
679   https://doi.org/10.1029/2017JD027711, 2018.

680 Van Marle, M. J. E., Kloster, S., Magi, B. I., Marlon, J. R., Daniau, A.-L., Field, R. D., Arneth,
681   A., Forrest, M., Hantson, S., Kehrwald, N. M., Knorr, W., Lasslop, G., Li, F., Mangeon, S.,
682   Yue, C., Kaiser, J. W., and Van Der Werf, G. R.: Historic global biomass burning emissions
683   for CMIP6 (BB4CMIP) based on merging satellite observations with proxies and fire models
684   (1750–2015), Geosci. Model Dev., 10, 3329–3357, https://doi.org/10.5194/gmd-10-3329-
685   2017, 2017.

686 Wang, B., Biasutti, M., Byrne, M. P., Castro, C., Chang, C.-P., Cook, K., Fu, R., Grimm, A. M.,
687   Ha, K.-J., Hendon, H., Kitoh, A., Krishnan, R., Lee, J.-Y., Li, J., Liu, J., Moise, A., Pascale,
688   S., Roxy, M. K., Seth, A., Sui, C.-H., Turner, A., Yang, S., Yun, K.-S., Zhang, L., and Zhou,
689   T.: Monsoons Climate Change Assessment, Bull. Am. Meteorol. Soc., 102, E1–E19,
690   https://doi.org/10.1175/BAMS-D-19-0335.1, 2021.

691 Wang, H., Easter, R. C., Rasch, P. J., Wang, M., Liu, X., Ghan, S. J., Qian, Y., Yoon, J.-H., Ma,
692   P.-L., and Vinoj, V.: Sensitivity of remote aerosol distributions to representation of cloud–
693   aerosol interactions in a global climate model, Geosci. Model Dev., 6, 765–782,
694   https://doi.org/10.5194/gmd-6-765-2013, 2013.

695 Wang, P., Yang, Y., Xue, D., Ren, L., Tang, J., Leung, L. R., and Liao, H.: Aerosols overtake
696   greenhouse gases causing a warmer climate and more weather extremes toward carbon
697   neutrality, Nat. Commun., 14, 7257, https://doi.org/10.1038/s41467-023-42891-2, 2023.

Wang, Z., Zhang, H., and Zhang, X.: Projected response of East Asian summer monsoon system to future reductions in emissions of anthropogenic aerosols and their precursors, Clim. Dyn., 47, 1455–1468, https://doi.org/10.1007/s00382-015-2912-7, 2016.

Wang, Z., Lin, L., Xu, Y., Che, H., Zhang, X., Zhang, H., Dong, W., Wang, C., Gui, K., and Xie, B.: Incorrect Asian aerosols affecting the attribution and projection of regional climate change in CMIP6 models, npj Clim. Atmos. Sci., 4, 2, https://doi.org/10.1038/s41612-020-00159-2, 2021.

Ward, M., Tulloch, A. I. T., Radford, J. Q., Williams, B. A., Reside, A. E., Macdonald, S. L., Mayfield, H. J., Maron, M., Possingham, H. P., Vine, S. J., O'Connor, J. L., Massingham, E. J., Greenville, A. C., Woinarski, J. C. Z., Garnett, S. T., Lintermans, M., Scheele, B. C., Carwardine, J., Nimmo, D. G., Lindenmayer, D. B., Kooyman, R. M., Simmonds, J. S., Sonter, L. J., and Watson, J. E. M.: Impact of 2019–2020 mega-fires on Australian fauna habitat, Nat. Ecol. Evol., 4, 1321–1326, https://doi.org/10.1038/s41559-020-1251-1, 2020.

Wasko, C., Shao, Y., Vogel, E., Wilson, L., Wang, Q. J., Frost, A., and Donnelly, C.: Understanding trends in hydrologic extremes across Australia, J. Hydrol., 593, 125877, https://doi.org/10.1016/j.jhydrol.2020.125877, 2021.

Yang, Y., Zeng, L., Wang, H., Wang, P., and Liao, H.: Climate effects of future aerosol reductions for achieving carbon neutrality in China, Sci. Bull., 68, 902–905, https://doi.org/10.1016/j.scib.2023.03.048, 2023.

Zacharakis, I. and Tsihrintzis, V. A.: Integrated wildfire danger models and factors: A review, Sci. Total Environ., 899, 165704, https://doi.org/10.1016/j.scitotenv.2023.165704, 2023.

Zeng, L., Yang, Y., Wang, H., Wang, J., Li, J., Ren, L., Li, H., Zhou, Y., Wang, P., and Liao, H.: Intensified modulation of winter aerosol pollution in China by El Niño with short duration, Atmos. Chem. Phys., 21, 10745–10761, https://doi.org/10.5194/acp-21-10745-2021, 2021.

Zhang, Q., Zheng, Y., Tong, D., Shao, M., Wang, S., Zhang, Y., Xu, X., Wang, J., He, H., Liu, W., Ding, Y., Lei, Y., Li, J., Wang, Z., Zhang, X., Wang, Y., Cheng, J., Liu, Y., Shi, Q., Yan, L., Geng, G., Hong, C., Li, M., Liu, F., Zheng, B., Cao, J., Ding, A., Gao, J., Fu, Q., Huo, J., Liu, B., Liu, Z., Yang, F., He, K., and Hao, J.: Drivers of improved PM2.5 air quality in China from 2013 to 2017, Proc. Natl. Acad. Sci., 116, 24463–24469, https://doi.org/10.1073/pnas.1907956116, 2019.

Zheng, B., Tong, D., Li, M., Liu, F., Hong, C., Geng, G., Li, H., Li, X., Peng, L., Qi, J., Yan, L., Zhang, Y., Zhao, H., Zheng, Y., He, K., and Zhang, Q.: Trends in China's anthropogenic emissions since 2010 as the consequence of clean air actions, Atmos. Chem. Phys., 18, 14095–14111, https://doi.org/10.5194/acp-18-14095-2018, 2018.

Zheng, Y., Xue, T., Zhang, Q., Geng, G., Tong, D., Li, X., and He, K.: Air quality improvements and health benefits from China's clean air action since 2013, Environ. Res. Lett., 12, 114020, https://doi.org/10.1088/1748-9326/aa8a32, 2017.

735   Zheng, Y., Zhang, Q., Tong, D., Davis, S. J., and Caldeira, K.: Climate effects of China's efforts
736   to improve its air quality, Environ. Res. Lett., 15, 104052, https://doi.org/10.1088/1748-
737   9326/ab9e21, 2020.

738

739
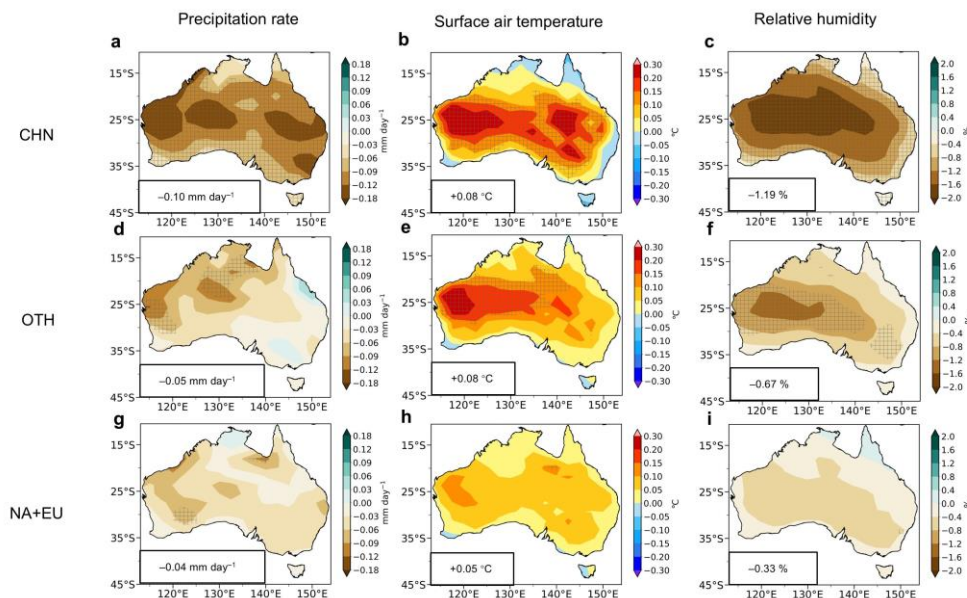
Figure 1. Simulated changes in precipitation rate, surface air temperature and relative humidity in Australia due to aerosol changes between 2013 and 2019. Spatial distributions of simulated differences in annual mean precipitation rate (Pr, **a, d,** and **g**, unit: mm day^{-1}), surface air temperature (TS, **b**, **e**, and **h**, unit: °C) and relative humidity (RH, **c, f**, and **i**, unit: %) in Australia between BASE and CHN (CHN minus BASE, **a**–**c**), between BASE and OTH (OTH minus BASE, **d**–**f**), and between BASE and NAEU (NAEU minus BASE, **g**–**i**). The shaded areas indicate results are statistically significant at the 90% confidence level. Regional averages over Australia are noted at the bottom-left corner of each panel.
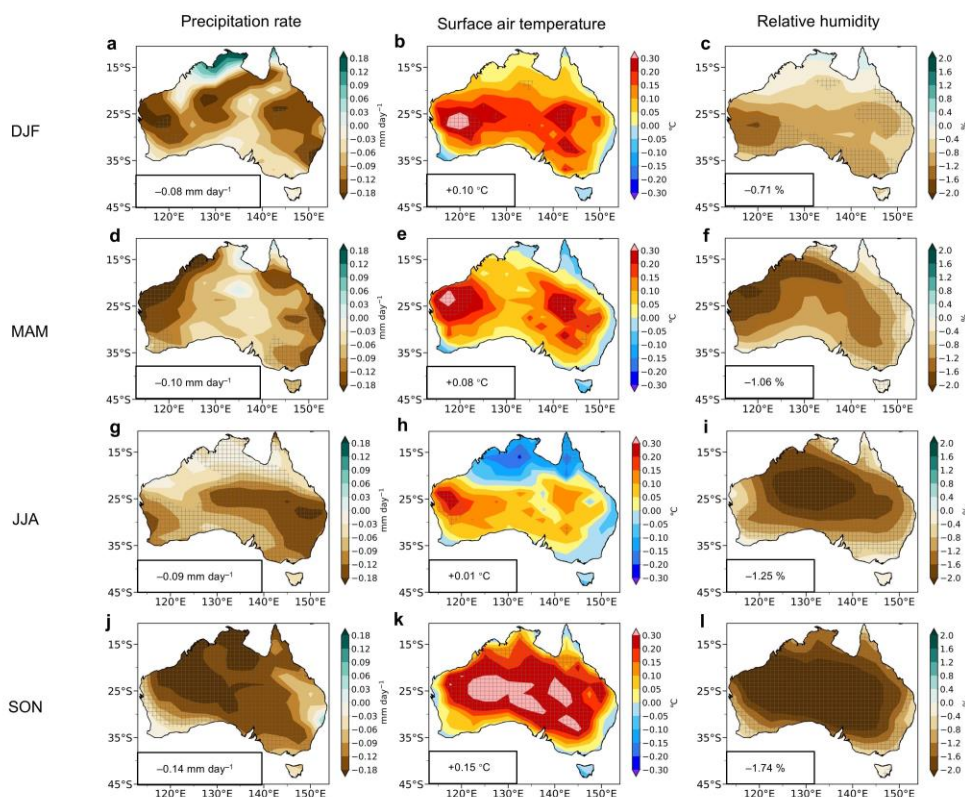
Figure 2. Simulated changes in precipitation rate, surface air temperature and relative humidity in Australia due to aerosol changes in China between 2013 and 2019. Spatial distributions of simulated differences in DJF (December, January and February, **a**–**c**), MAM (March, April and May, **d**–**f**), JJA (June, July and August, **g**–**i**) and SON (September, October and November, **j**–**l**) mean precipitation rate (Pr, **a**, **d**, **g**, and **j**, unit: mm day^{-1}), surface air temperature (TS, **b**, **e**, **h**, and **k**, unit: °C) and relative humidity (RH, **c**, **f**, **i**, and **l**, unit: %) in Australia between BASE and CHN (CHN minus BASE).The shaded areas indicate results are statistically significant at the 90% confidence level. Regional averages over Australia are noted at the bottom-left corner of each panel.

759
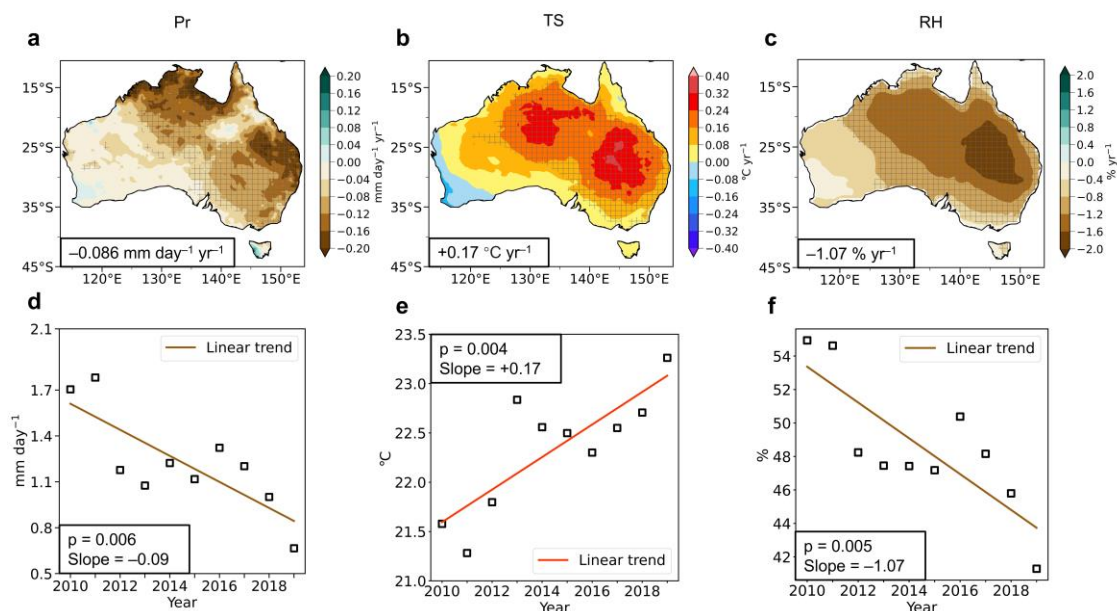
Figure 3. Linear trends of observed precipitation rate, surface air temperature and relative humidity in Australia based on ERA5. Spatial distributions of linear trends (**a**, **b**, and **c**) and time series (**d**, **e**, and **f**) of annual mean precipitation rate (Pr, **a** and **d**, unit: mm day^{-1}), surface air temperature (TS, **b** and **e**, unit: °C) and relative humidity (RH, **c** and **f**, unit: %) in Australia during 2010–2019 from ERA5 reanalysis. The shaded areas indicate trends are statistically significant at the 90% confidence level. Regional averages over Australia are noted at the bottom-left corner of panels a, b, and c. The p values and slopes of linear trends are noted in panels d, e, and f.

767

768
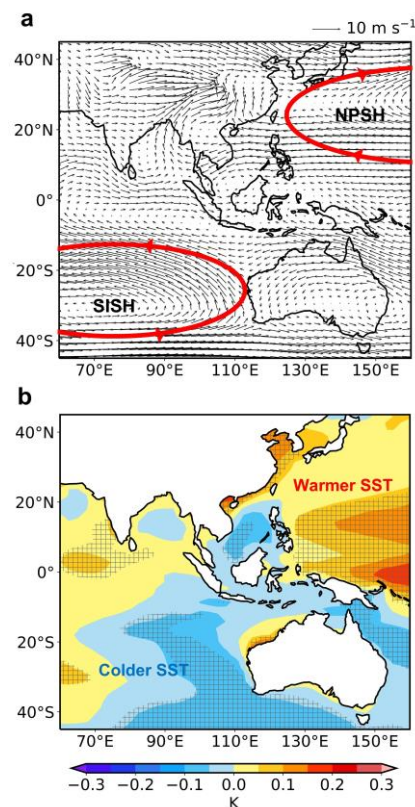
Figure 4. Climatological mean wind fields at 850 hPa and Simulated sea surface temperature changes due to aerosol changes in China between 2013 and 2019. a, Climatological mean wind fields (unit: m s^{-1}, vectors) at 850 hPa from the BASE experiment. NPSH and SISH shown in red circles represents North Pacific Subtropical High and Southern Indian ocean Subtropical High, respectively. **b**, Spatial distributions of simulated differences in annual mean sea surface temperature (SST, unit: mm day^{-1}) in Australia between BASE and CHN (CHN minus BASE). The shaded areas indicate results are statistically significant at the 90% confidence level.

776

777
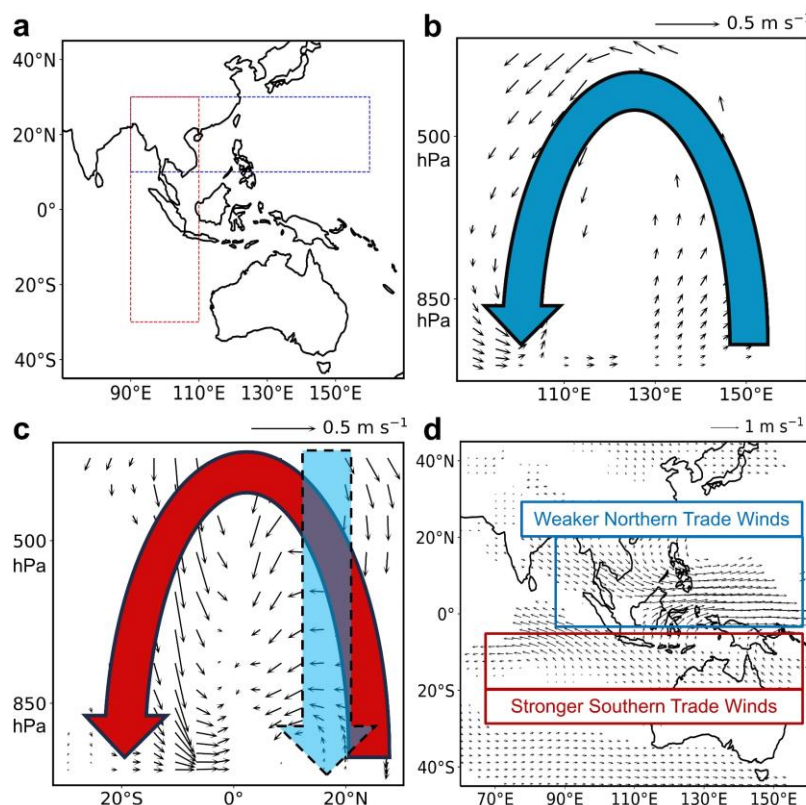
Figure 5. Simulated changes in vertical circulations and 850 hPa wind fields in Asia-Pacific

regions due to aerosol changes in China between 2013 and 2019. Panel **b** and **c** shows pressure–
longitude and pressure–latitude cross-section of responses in annual mean atmospheric
circulations (unit: m s^{-1}, vectors), respectively, over the areas marked with the blue and red box in
panel **a**. Panel **d** shows annual mean changes in wind fields (unit: m s^{-1}, vectors) at 850 hPa in
Asia-Pacific regions. Only atmospheric circulations and winds statistically significant at the 90%
confidence level are shown.

785
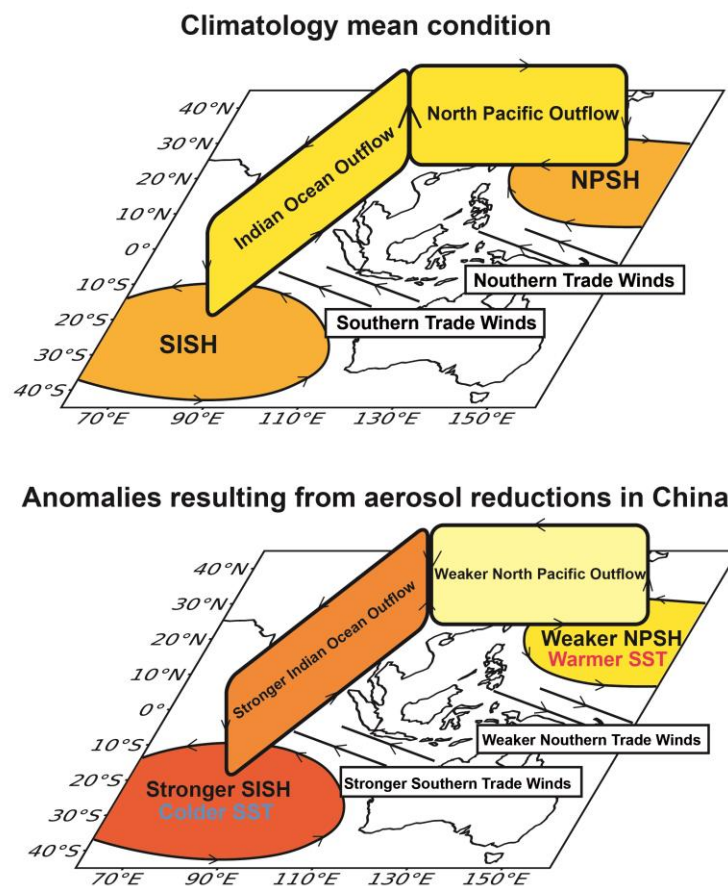
Figure 6. Schematic of the response in large-scale 3D circulations in the Asian-Pacific region to aerosol reductions in China. The top panel shows climatology mean condition, and the bottom panel shows anomalies resulting from aerosol reductions in China.

790
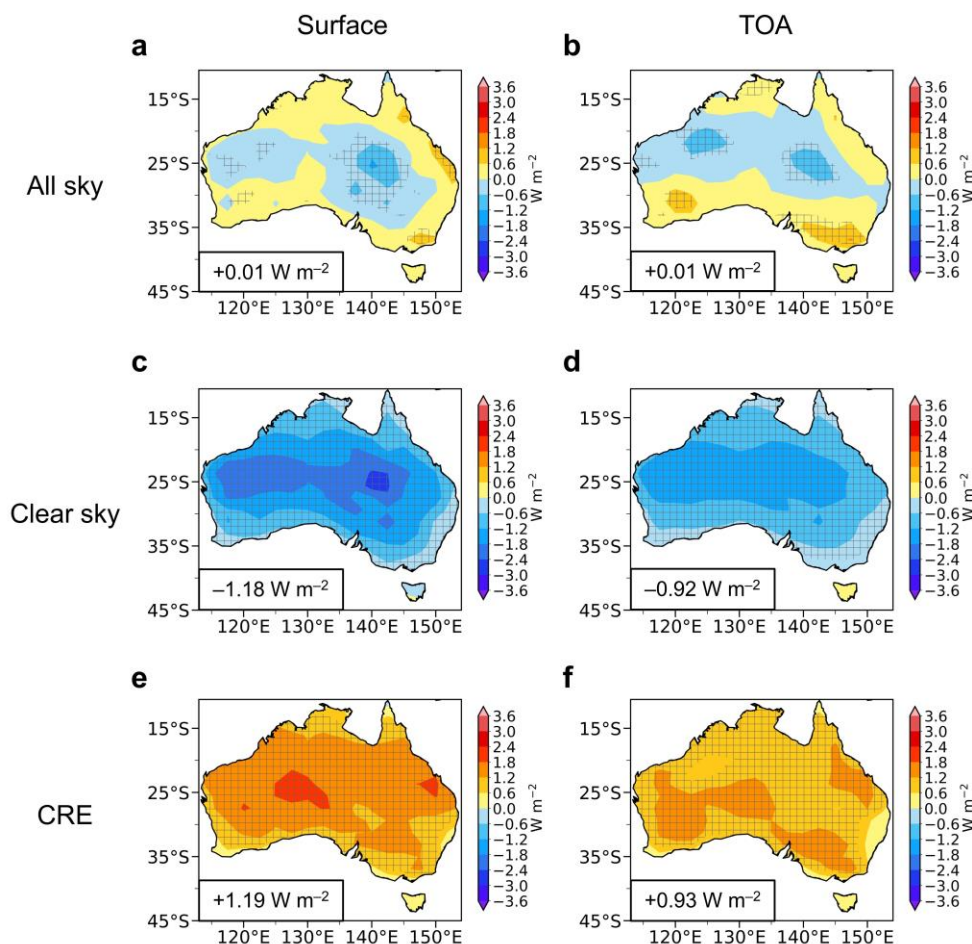
Figure 7. Simulated changes in surface and Top of the Atmosphere (TOA) net total radiative flux under all sky conditions, under clear sky conditions, and from cloud radiative effects in Australia due to aerosol changes in China between 2013 and 2019. Spatial distributions of simulated differences in annual mean surface (**a**, **c**, and **e**) and Top of the Atmosphere (TOA, **b**, **d**, and **f**) net total radiative flux (unit: W m^{-2}) under all sky conditions (**a** and **b**), under clear sky conditions (**c** and **d**), and from cloud radiative effects (CRE, **e** and **f**) in Australia between BASE and CHN (CHN minus BASE). Cloud radiative effects refer to differences under all sky and clear sky conditions (All sky minus Clear sky). The shaded areas indicate results are statistically significant at the 90% confidence level. Regional averages of the responses over Australia are noted at the bottom-left corner of each panel.

801
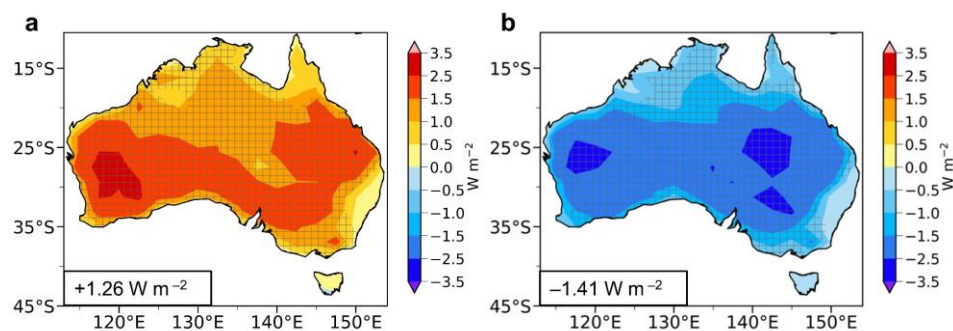
Figure 8. Simulated changes in surface upward sensible and latent heat flux in Australia due to aerosol changes in China between 2013 and 2019. Spatial distributions of simulated differences in annual mean surface upward sensible (**a**) and latent (**b**) heat flux (unit: W m^{-2}) in Australia between BASE and CHN (CHN minus BASE). The shaded areas indicate results are statistically significant at the 90% confidence level. Regional averages over Australia are noted at the bottom-left corner of each panel.
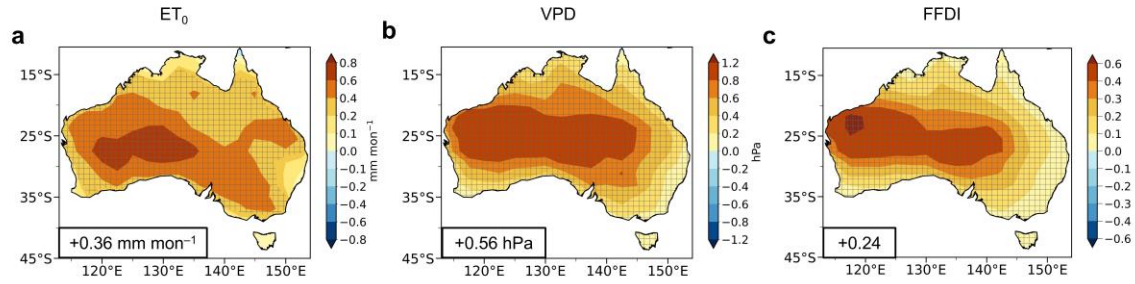
Figure 9. Simulated changes in reference potential evapotranspiration, vapor pressure deficit, and McArthur forest fire danger index during fire seasons in Australia due to aerosol changes in China between 2013 and 2019. Spatial distributions of simulated changes in reference potential evapotranspiration (ET$_0$, **a**, unit: mm mon^{-1}), vapor pressure deficit (VPD, **b**, unit: hPa), and McArthur forest fire danger index (FFDI, **c**, unitless) during fire seasons (austral spring and summer, from September to the February of the next year) in Australia between BASE and CHN (CHN minus BASE). The shaded areas indicate results are statistically significant at the 90% confidence level. Regional averages over Australia are noted at the bottom-left corner of each panel.